J. Fluid Mech. (1994), *vol.* 272, *pp.* 67–89

Plume formation and resonant bifurcations in porous-media convection

By MICHAEL D. GRAHAM[1] AND PAUL H. STEEN[2]

[1] Department of Chemical Engineering, University of Wisconsin, Madison, WI 53706–1691, USA

[2] School of Chemical Engineering, and Center for Applied Mathematics, Cornell University, Ithaca, NY 14853–5204, USA

(Received 28 May 1993 and in revised form 2 February 1994)

The classical boundary-layer scaling laws proposed by Howard for Rayleigh–Bénard convection at high Rayleigh number extend to the analogous case of convection in saturated porous media. We computationally study two-dimensional porous-media convection near the onset of this scaling behaviour. The main result of the paper is the observation and study of instabilities that lead to deviations from the scaling relations.

At Rayleigh numbers below the scaling regime, boundary-layer fluctuations born at a Hopf bifurcation strengthen and eventually develop into thermal plumes. The appearance of plumes corresponds to the onset of the boundary-layer scaling behaviour of the oscillation frequency and mean Nusselt number, in agreement with the classical theory. As the Rayleigh number increases further, the flow undergoes instabilities that lead to 'bubbles' in parameter space of quasi-periodic flow, and eventually to weakly chaotic flow. The instabilities disturb the plume formation process, effectively leading to a phase modulation of the process and to deviations from the scaling laws. We argue that these instabilities correspond to parametric resonances between the timescale for plume formation and the characteristic convection timescale of the flow.

1. Introduction

Simulations of buoyancy-driven convection in containers of fluid-saturated porous material heated from below display sequences of flows proceeding from stationary to chaotic, as the overall temperature difference is increased (Kimura, Schubert and Straus 1986, 1989; Caltagirone & Fabrie 1989; Graham & Steen 1992). As with the case of classical pure fluid convection, the time-dependent behaviour can be identified with that expected from a low-dimensional dynamical system. Questions still remain, however, about the fluid mechanics associated with these transitions, and in particular, the relationship to the classical asymptotic scaling laws first put forth by Howard (1964) on the basis of physical and dimensional arguments. We address these questions in the context of two-dimensional flows in a square container of fluid-saturated porous material, discussing both the onset of the scaling behaviour and deviations from it. In the present case, these deviations are in fact a result of instability of a simple time-periodic flow that obeys the classical scaling laws.

The regime studied here is the beginning of the 'high Rayleigh number' regime, where convection is dominated by buoyancy and molecular diffusion plays little part in the bulk of the flow. Consider for the moment the pure fluid case, on which most classical analyses concentrate. A dimensional analysis that neglects diffusion altogether predicts

$$\overline{Nu} \sim R^{\frac{1}{2}},$$

where $\overline{Nu}$ is the mean Nusselt number and R the Rayleigh number, or dimensionless temperature difference. The exponent in this expression is much higher than that found in experiments. The reason for the discrepancy is the presence of thermal boundary layers at the top and bottom surfaces. The assumption of the existence of a lengthscale, the boundary-layer thickness δ, that is independent of the height, l, of the box gives

$$\overline{Nu} \sim R^{\frac{1}{3}}.$$

A more detailed analysis, presented by Howard (1964) extends this simple boundary-layer argument and captures much of the basic physics of convection at high R. In his model, the fluid and boundaries are initially motionless and isothermal. At time $t = 0$, the top and bottom boundaries are impulsively heated to $\pm\frac{1}{2}\Delta T$. Consider what happens at the bottom boundary. Initially no motion occurs and the transient conduction profile develops:

$$T(z) = \tfrac{1}{2}\Delta T \operatorname{erfc}\left(\frac{z}{(4\kappa t)^{\frac{1}{2}}}\right),$$

where κ is the thermal diffusivity of the fluid. At a critical time t^*, this boundary layer destabilizes and plumes of warm fluid form, which suck fluid away from the boundary. This plume formation and release stage is assumed to be short compared to t^*, and to strip the surface entirely of warm fluid, so the conduction phase recurs. Because the instability occurs so quickly (by hypothesis) the conduction phase dominates the behaviour in the boundary layer, and thus the heat transfer through the entire layer. Let $\delta^* \equiv (\pi\kappa t^*)^{\frac{1}{2}}$ be a measure of the critical boundary-layer thickness and R_{δ^*} be the Rayleigh number based on this thickness. The mean Nusselt number is dominated by conduction through the layer, so

$$\overline{Nu} \sim \frac{l}{\delta^*} \sim \left(\frac{R}{R_{\delta^*}}\right)^{\frac{1}{3}}. \tag{1}$$

The critical time t^* is as yet unknown, but its scaling behaviour can be found:

$$t^* \sim \delta^{*2} \sim R^{-\frac{2}{3}},$$

or

$$f^* = \frac{1}{t^*} \sim R^{\frac{2}{3}}, \tag{2}$$

where f^* is the characteristic frequency of plume formation. These scaling laws have been observed in experiments (Krishnamurti 1970; Turner 1973), although in general, the observed exponents are somewhat lower than those arising from this simple analysis. In the porous medium, the mechanism is the same, but since R scales linearly with l instead of cubically, the scaling laws become

$$\overline{Nu} \sim R, \tag{3}$$

$$f^* \sim R^2, \tag{4}$$

(Horne & O'Sullivan 1978) and are the foundation for the results in the present work. These scaling laws are also observed in experiments in porous media (Elder 1967; Buretta 1972) and Hele-Shaw cells (Koster & Müller 1982). We note that experiments in pure fluid convection at very high R (the so-called 'hard turbulence' regime) display significant deviations from the classical scaling discussed here. These deviations are attributable to interaction between the boundary layers and the turbulent bulk flow (Castaing *et al.* 1989).

Howard argues that the rate limiting step in the instability of the boundary layer is

essentially a Rayleigh–Bénard phenomenon, so t^* is determined by the critical thickness for this instability. However, he presents no detailed analysis of the instability. Foster (1965) performs numerical experiments on the linearized problem and finds that the instability does grow rapidly, verifying the assumption of the model. He also finds the predicted scaling, but does not discuss the mode of instability. Elder (1968) extends this work, studying numerically both the pure fluid and porous medium. He observes that flow occurs first within the boundary layer and only later do plumes burst from the layer. Thus the initial instability is indeed Rayleigh–Bénard-like. R_{δ^*} is a critical Rayleigh number for a Rayleigh–Bénard problem and t^* is the time required to reach this Rayleigh number. The instability grows rapidly and eventually buoyancy dominates diffusion and plumes form and rise, drawing warm fluid out of the boundary layers, thereby keeping them thin. This latter stage is essentially a Rayleigh–Taylor flow in which diffusion plays little or no role. A simple extension of this model considers a uniform flow right to left over a horizontal plate heated only in the left half. Here the thermal boundary layer develops spatially instead of temporally.

Kimura *et al.* (1986; hereinafter referred to as KSS) and Caltagirone & Fabrie (1989; hereinafter referred to as CF) report computational results for two-dimensional convection in a square of porous medium at Rayleigh numbers high enough for the asymptotic scalings to be observed. KSS find that between $R = 550$ and $R = 1100$, the following scalings are observed:

$$\overline{Nu} \sim R^{\frac{11}{10}}, \quad f_1 \sim R^{\frac{3}{2}}.$$

The large deviation in f_1 from the asymptotic scaling of R^2 is due to their inclusion of data at low R, where the scaling is clearly not observed (cf. their figure 2). At $R = 1000$, they find two chaotic states with different dominant frequencies. Below, we show solutions with similar frequencies, but no broadband behaviour; the chaos they observe is an artefact of insufficient spatial resolution. The results of CF are in agreement with ours and those of KSS through $R = 600$. At $R = 800$ and 1000, the frequencies remain in good agreement, but the mean Nusselt numbers are consistently high. Furthermore, their frequency spectra are difficult to interpret, as the baselines are only two decades below the highest peaks, making any weak chaos or quasi-periodicity invisible. It is possible that they have jumped to different solutions. Having made these caveats, we note that the asymptotic frequency scaling fits roughly through their results. They find three-frequency behaviour at $R = 1000$ and $R = 1200$, and chaos at $R = 1350$ and $R = 1500$. At higher R, the single roll mean flow breaks down as plumes invade the interior of the flow.

We computationally study the regime from $R = 600$ to 1250 in the square of saturated porous medium. The dominant behaviour in this regime centres on the time-periodic flow born at a Hopf bifurcation (convected boundary-layer instability) from the steady roll pattern at $R = 544$ (cf. Graham & Steen 1992; hereinafter referred to as GS) and subsequent bifurcations from this periodic flow. Figure 1 is a schematic bifurcation diagram that places the regime of interest in the larger context. Following the conduction and steady regime of interest in the larger context. Following the conduction and steady convection regimes is a 'travelling wave' regime. Travelling waves are time-periodic boundary-layer fluctuations with spatial wavenumber n, each born at a Hopf bifurcation. Modal interactions of these waves lead to quasi-periodic mixed modes (the quasi-periodic branches are not shown on figure 1). GS focuses on the latter regime which ends where the regime of interest in this paper begins. The remainder of this paper is devoted to explaining the details of the scaling regime shown schematically in figure 1.

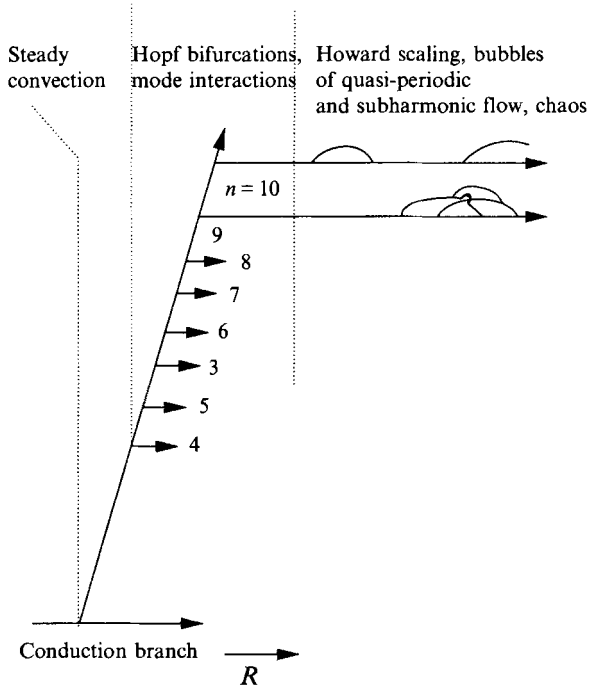

FIGURE 1. Overall bifurcation diagram, from conduction to steady convection to weakly interacting periodic fluctuations to the Howard scaling regime studied in this paper ($R \approx 700$–1200). Wavenumbers of boundary-layer fluctuations are denoted by n.

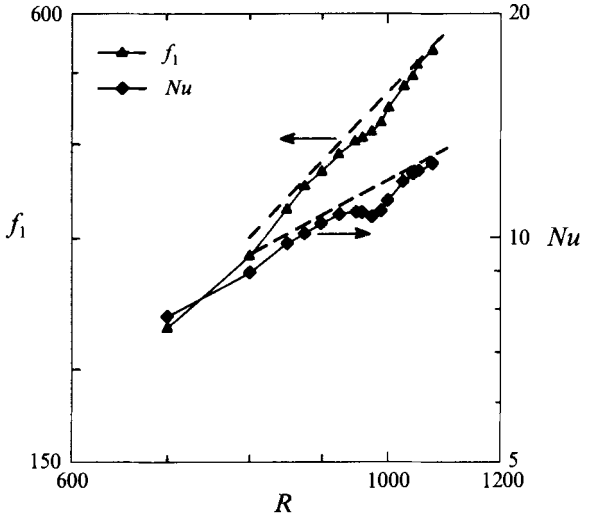

FIGURE 2. $\overline{Nu}$ and f_1 *vs.* R on the centrosymmetric branch originating at the birth of the $n = 9$ periodic flow. Dashed curves indicate the boundary layer scaling laws discussed in the text.

Figure 2 provides a guide for the outline of the paper. It shows results of initial-value problems in the regime $600 < R < 1050$. We discuss first the onset of asymptotic scaling, which occurs near $R = 700$, when fluctuations in the boundary layers reach sufficient strength to form plumes. Compare the results on figure 2 with the dashed lines representing the asymptotic scaling laws, equations (3) and (4). Above the onset

of scaling, the periodic flow undergoes a number of bifurcations leading to 'bubbles' of quasi-periodic flow. The deviation from asymptotic scaling between $R = 950$ and $R = 1050$ on figure 2 corresponds to one such bubble. The classical fluid dynamical example leading to such bifurcation behaviour is the instability of a horizontal fluid layer in a vertically vibrating tray, first studied by Faraday (see Drazin & Reid 1981). The linear stability problem for this system reduces to a Mathieu equation, the classical example of a parametrically forced system. However, the destabilizing forcing is imposed externally in the Faraday problem, whereas here the excitation arises internally, from the periodic plume formation and convective processes themselves. Using the scaling laws and equations for fluctuations from the periodic flow, we discuss the dominant balances that govern the instability. At $R = 1200$ and $R = 1250$, weakly chaotic solutions are found. The spatial behaviour in this regime is essentially similar to that in the quasi-periodic regimes at lower R.

2. Governing equations and computational techniques

Consider a closed, square box of height l, filled with a fluid-saturated porous medium (Joseph 1976). Flow within is described by Darcy's law and the inertia terms are neglected (i.e. the dimensionless permeability $K = k/l^2$ of the medium is assumed to be very small). The horizontal top and bottom are isothermal with the bottom warmer than the top; when no motion occurs, a linear temperature gradient is present in the medium. The vertical walls are adiabatic. The buoyancy of the fluid is described by the Oberbeck–Boussinesq approximation; the variable density of the fluid is retained only in the body force term of the momentum equation. All other physical properties are constant. Under these conditions, the dimensionless equations for deviations from the linear thermal conduction profile $T_0 = \frac{1}{2} - z$ are

$$\left.\begin{aligned} \nabla\cdot\boldsymbol{v} &= 0, \\ \mathbf{0} &= -\nabla p - \boldsymbol{v} + R\theta\boldsymbol{k}, \\ \frac{\partial\theta}{\partial t} + \boldsymbol{v}\cdot(\nabla\theta - \boldsymbol{k}) &= \nabla^2\theta \\ \nabla\theta\cdot\boldsymbol{n} &= 0 \quad \text{on sidewalls,} \quad x = \pm\tfrac{1}{2}, \\ \theta &= 0 \quad \text{on top and bottom,} \quad z = \pm\tfrac{1}{2}, \\ \boldsymbol{v}\cdot\boldsymbol{n} &= 0 \quad \text{on all boundaries,} \end{aligned}\right\} \tag{5}$$

where $\boldsymbol{v}, p$ and θ are the velocity, pressure and temperature deviations, respectively. The Rayleigh number is $R = g\alpha\Delta T k l/\kappa_m \nu$ where α is the coefficient of thermal expansion of the fluid, g is the magnitude of gravity, ΔT is the temperature difference between bottom and top, ν is the kinematic viscosity and κ_m is an effective thermal diffusivity of the fluid–solid mixture. The scales are, for velocity κ_m/l, temperature ΔT, length l and time $l^2 C/\kappa_m$, where C is the ratio of volumetric heat capacity of the saturated medium to that of the fluid. In terms of the formulation given here, the instantaneous dimensionless heat transfer rate, or Nusselt number, Nu, is given by:

$$Nu(t) = 1 - \int_{-\frac{1}{2}}^{\frac{1}{2}} \left.\frac{\partial\theta(x,z,t)}{\partial z}\right|_{z=-\frac{1}{2}} \mathrm{d}x, \tag{6}$$

and the mean Nusselt number $\overline{Nu}$ is:

$$\overline{Nu} = \lim_{T\to\infty} \frac{1}{T}\int_0^T Nu(t)\,\mathrm{d}t. \tag{7}$$

It is convenient to reformulate (5) as a single integro-differential equation for θ (Steen 1986); the scalar temperature field determines the velocity field uniquely. The energy equation can be rewritten:

$$\frac{\partial\theta}{\partial t}+(-\nabla p+R\theta\boldsymbol{k})\cdot(\nabla\theta-\boldsymbol{k})=\nabla^2\theta. \tag{8}$$

Taking the divergence of the momentum equation and applying continuity leaves a Poisson equation with Neumann boundary conditions for the pressure:

$$\nabla^2 p = R\nabla\theta\cdot\boldsymbol{k}. \tag{9}$$

This equation can be inverted to give an integral equation for p in terms of θ and the result inserted into (8).

It is often desirable to enforce the restriction of 'centrosymmetry' to study solutions that are otherwise unstable. Centrosymmetric solutions satisfy:

$$\theta(x,z)=-\theta(-x,-z), \tag{10}$$

or in terms of the original temperature field $T(x,y)$:

$$T(x,z)=1-T(-x,-z). \tag{11}$$

Computations for this study use primarily the initial-value problem (IVP). A pseudo-spectral collocation formulation is used for spatial discretization of the governing equations (8) and (9). Chebyshev polynomials are used in the vertical direction and trigonometric functions in the horizontal. Chebyshev polynomials are chosen because of their ability to resolve boundary layers more efficiently than trigonometric polynomials (see e.g. Canuto *et al.* 1988; Boyd 1989). The techniques used here are standard and will not be discussed in detail. Differentiation of the approximate solution can be performed two ways: by transforming from physical to spectral space and using a recurrence relation for differentiation of Chebyshev polynomials, or by use of a matrix operator (given in Canuto *et al.* 1988) relating a quantity and its derivative directly. The latter form is preferred when the Jacobian is desired (as when performing parameter continuation), but the former may be more efficient because FFTs can be used to flip from physical to spectral space and vice versa. Authors differ on which technique is more efficient on vector processors (Fornberg 1990; Canuto *et al.* 1988); the matrix multiplication form is used here.

Dirichlet boundary conditions are applied by simply setting $\theta_0=\theta_N\equiv 0$, where θ_i is the solution at the ith collocation point (considering for the moment only one dimension). Neumann boundary conditions can be applied implicitly by modifying the differentiation matrix $\boldsymbol{D}$ such that $D_{0j}\theta_j=D_{Nj}\theta_j=0$. This formulation does not satisfy the boundary conditions exactly, but the error decays spectrally (Canuto *et al.* 1988).

For time discretization, a second-order accurate operator splitting method is used. The convective portion of the energy equation is advanced explicitly, using a second-order Adams formula:

$$\frac{\theta^*-\theta^n}{\Delta t}=-\tfrac{3}{2}((\nabla p^n+R\theta^n\boldsymbol{k})\cdot(\nabla\theta^n-\boldsymbol{k}))+\tfrac{1}{2}((\nabla p^{n-1}+R\theta^{n-1}\boldsymbol{k})\cdot(\nabla\theta^{n-1}-\boldsymbol{k})). \tag{12}$$

The superscripts represent the timesteps. The asterisk represents an intermediate solution. An eigenvalue–eigenvector decomposition is used to solve the Poisson equation (9) for the pressure (Haidvogel & Zang 1979). Most of the work in this step can be performed in a preprocessing step, so only $O(N^2)$ operations are required at

each timestep. The timestep is completed with a Crank–Nicholson step for the Laplacian:

$$\frac{\theta^{n+1}-\theta^*}{\Delta t} = \nabla^2\left(\frac{\theta^{n+1}+\theta^*}{2}\right). \tag{13}$$

This can also be solved by the eigenvalue–eigenvector decomposition.

Spatial resolution has been checked carefully; all of the results presented are insensitive to changes in resolution. The results for $900 < R < 1050$ are from simulations with 64 Fourier modes in the horizontal direction and 48 Chebyshev in the vertical and timestep $\Delta t = 5 \times 10^{-6}$. Simulations at higher R use 72 or 84 Fourier modes.

As a supplement to some of the IVP computations, pseudo-arclength continuation with the subroutine package AUTO (Doedel 1981) is used to compute periodic solutions and their bifurcations. Details of the implementation can be found in GS.

3. Review of behaviour at low and intermediate R

Figure 1 shows a schematic bifurcation diagram. When $R < 4\pi^2$, all disturbance decay to the linear thermal conduction profile $\theta = 0$. This solution is globally stable (Beck 1972). The two-dimensional unicellular (single roll) flow in which we are interested is born at a pitchfork bifurcation at $R = 4\pi^2$. This steady flow remains stable until $R = 382$, when convected fluctuations in the thermal boundary layers near the top and bottom of the containers destabilize the steady state in a Hopf bifurcation. Just above this bifurcation a stable time-periodic state is found. The destabilizing thermal fluctuation can be assigned a wavenumber $n = 4$, the number of pairs of extrema of disturbance structure. At slightly higher R, this flow becomes unstable with respect to fluctuations with wavenumber $n = 5$, which is the first wavenumber to bifurcate if centrosymmetry is enforced (KSS; Aidun & Steen 1986, 1987). As R is increased further, the (now unstable) steady flow exhibits a sequence of Hopf bifurcations, each corresponding to a convected boundary-layer instability of a particular integer wavenumber (Steen & Aidun 1988; GS). At each transition, the frequency is proportional to the wavenumber and the velocity of the steady circulation. The observed stable time-dependent behaviour in the regime $400 < R < 700$ consists of overlapping intervals of periodic and quasi-periodic (two-frequency) behaviour (KSS; GS). At the end of this regime, the $n = 9$ periodic flow is stable. It can be shown that all of this behaviour arises from mode interactions between the various limit cycles born at the Hopf bifurcations (GS). The quasi-periodic flows are essentially nonlinear superpositions of a steady state and two time-periodic fluctuations of different wavenumbers. In a sense, then, all of the dynamics below $R = 700$ occur 'close' to the original steady unicellular solution and its Hopf bifurcations.

4. Boundary-layer scaling and plume formation

When $R > 606$, near the end of the regime just discussed, the $n = 9$ limit cycle is stable. This branch is where the present study begins. Above $R = 700$, until it becomes unstable at about $R = 950$, the $n = 9$ solution obeys to a good approximation the asymptotic scaling laws for time dependence and heat transfer predicted by Howard's theory. We discuss in this section the onset of scaling. The actual least squares curve fits, for results between $R = 700$ and 925 are $f \sim R^{1.95}$, $Nu \sim R^{1.15}$; the variances for the exponents are 0.33 and 0.21, respectively. Figure 2 shows how the frequency and mean Nusselt number change as R increases. The dashed line show the slopes of the

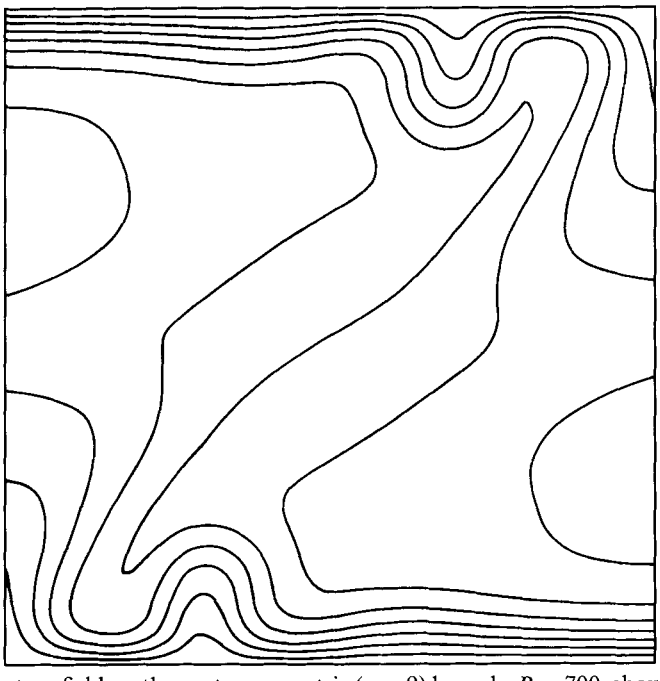

FIGURE 3. Temperature field on the centrosymmetric ($n = 9$) branch, $R = 700$, showing the formation of a plume. In this figure, and in figures below, the overall circulation of the flow is clockwise. In this figure, and in all figures showing contours of the total temperature field, the interval between contour levels is 0.1.

asymptotic laws, indicating how well these laws match the data. For clarity, the results in this figure are from solutions restricted to centrosymmetry. In the following sections we relax this restriction. Recall that at the Hopf bifurcation, the frequency is proportional to the steady circulation velocity, so that Howard scaling is not expected near the transition. The abrupt deviation from scaling at $R = 950$ corresponds to a quasi-periodic flow that we analyse §5.

One of the key elements in the physics of the asymptotic theory is the formation of thermal plumes, as fluctuations born in the boundary layer grow and eventually move fluid out of the boundary layer. Thus we expect to see plumes forming in this region of scaling behaviour. At the onset of this oscillation at $R = 544$, the fluctuations are infinitesimal, growing as they are convected across the horizontal isothermal surfaces. These fluctuations grow to greater strength as R increases. By about $R = 615$, a warm blob in the bottom boundary layer is just beginning to form a plume as it reaches the downstream end of the layer (and correspondingly a cold plume is forming in the top boundary layer). As an operational definition, we say that a plume has formed when an isotherm in the boundary layer has buckled to the extent that some portion of it becomes nearly vertical (away from the downstream corner). By $R = 700$, the plume forms far enough upstream to be distinct from the turning region in the corner (see figure 3) whereas at $R = 900$, the plume forms at about the centre of the layer. The Howard scaling begins to be valid above about $R = 700$, so as expected, the condition for this scaling is the formation of distinct plumes. Figure 4 shows one period of the temperature field at $R = 900$, showing the plume progression. What we see here is essentially the spatially developing version of the process described by Elder (1968); plume formation and thus Howard scaling does not occur until the fluctuations grow rapidly enough to reach the Rayleigh–Taylor stage before being convected out of the

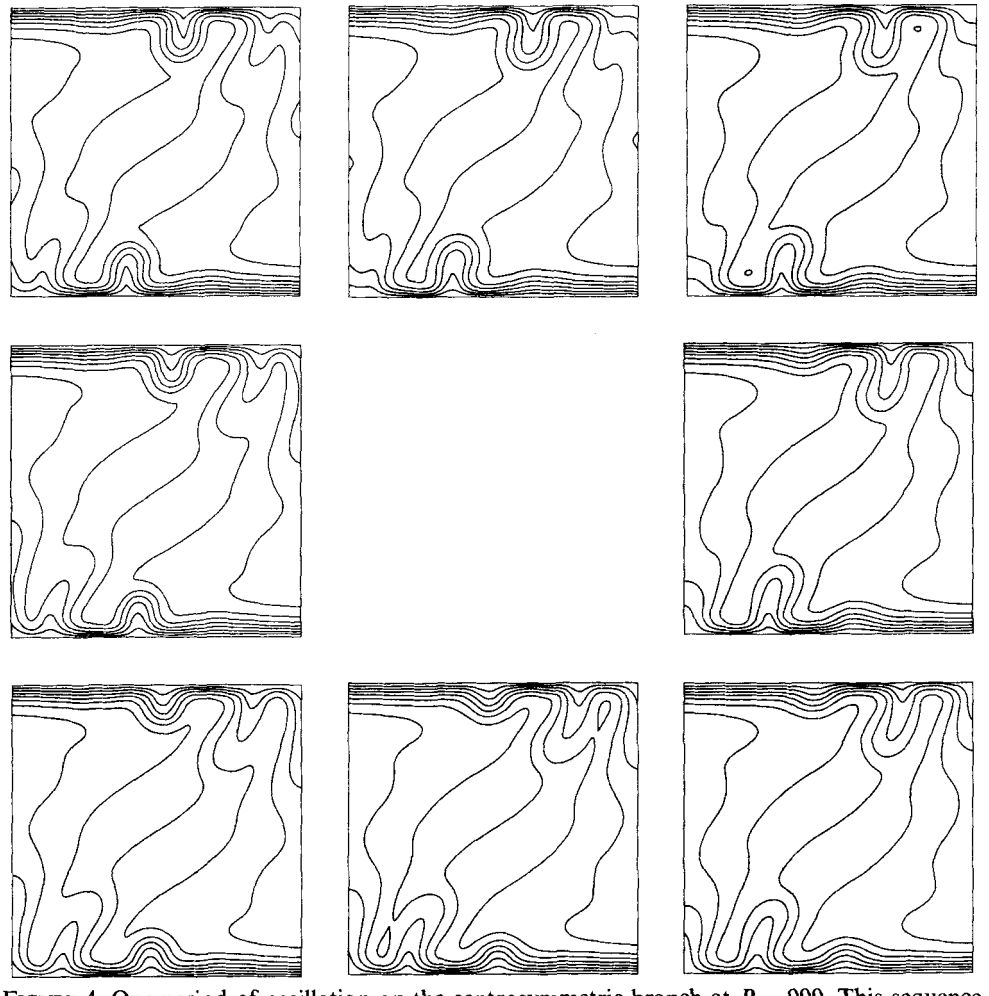

FIGURE 4. One period of oscillation on the centrosymmetric branch at $R = 900$. This sequence shows temperature T through the entire plume formation process. Time proceeds clockwise.

downstream corner of the boundary layer. During this gradual transition, there is no change in the dynamical picture of the solution; it is still a limit cycle, but the formation of plumes represents an important physical effect.

Between $R = 800$ and $R = 850$, another manifestation of the boundary-layer behaviour appears, as the wavenumber of the fluctuating part of the temperature field $\hat{T}$ increases from $n = 9$ to $n = 11$. This fluctuating part is defined as

$$\hat{T}(x, z, t) = T(x, z, t) - \int_0^{1/f_1} T(x, z, t)\,\mathrm{d}t.$$

The transition arises as an extremely small, weak blob appears at the upstream end of boundary layer; one blob becomes three. Figure 5 shows snapshots of the fluctuation at $R = 800$ and $R = 850$. The evolution of the pattern is smooth; no bifurcations occur. This transition is a consequence of the boundary-layer mechanism at work at these high Rayleigh numbers. The boundary-layer thickness δ scales as R^{-1}. Since the Rayleigh–Bénard mechanism drives the fluctuations, their wavelength λ scales as δ and therefore as R^{-1}. Thus the wavenumber is expected to increase with R. In a container, the wavenumber is quantized, so the scaling cannot be observed exactly. Nevertheless,

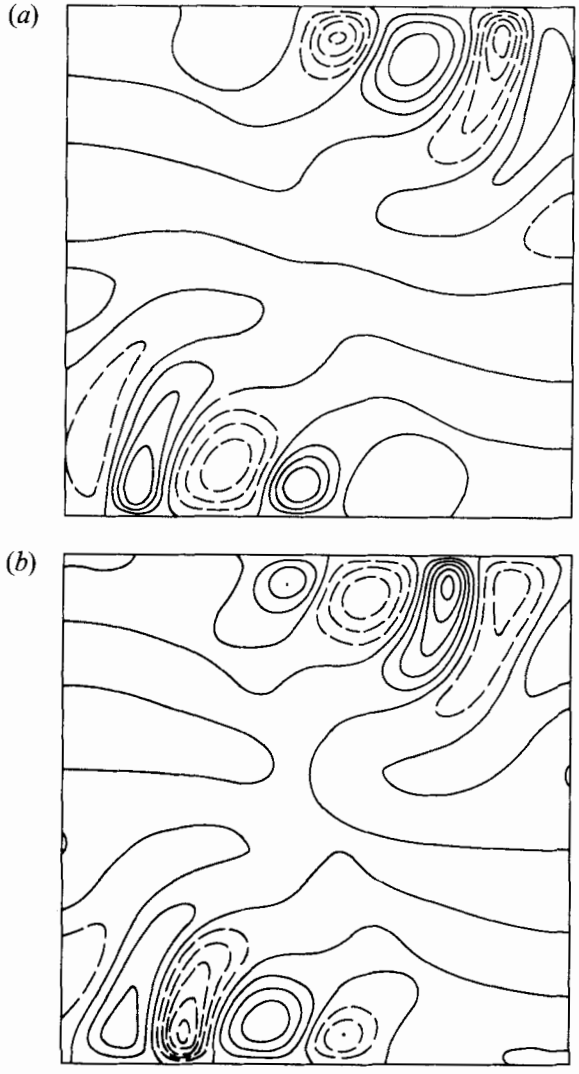

FIGURE 5. Snapshots of instantaneous temperature fluctuations $\hat{T}$ from the mean field at $R = 800$ (*a*) and 850 (*b*) on the centrosymmetric branch, showing the change in wavenumber from 9 to 11. Wavenumber is computed as one-half the number of sign changes in the fluctuation field around the perimeter of the container. The contour interval for plots of fluctuation fields varies from figure to figure, depending on the amplitude of the fluctuation.

the transition from one wavenumber to another can be smooth, as the additional fluctuations appear at infinitesimal amplitude. The distance of the plume breakoff point from the upstream corner also scales as R^{-1} in the asymptotic theory, and we find in the simulations that as R increases, the plumes form further upstream, in qualitative agreement with the theory.

5. Instabilities and deviations from scaling

The major subject of this work is the behaviour at Rayleigh numbers above the onset of the Howard scaling. This section centres on the instabilities that disrupt the scaling behaviour and how they are related to the underlying physics of the plume formation

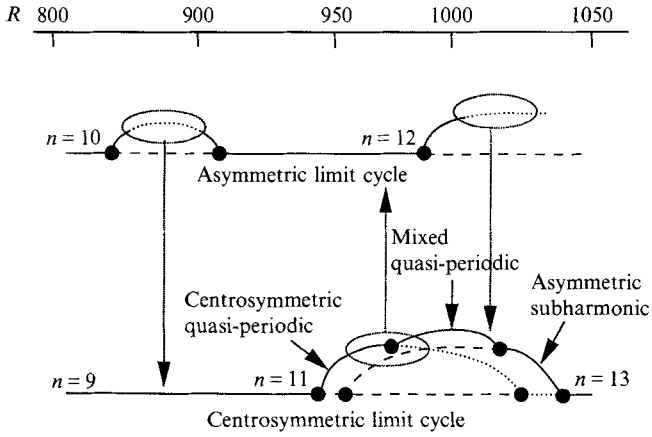

FIGURE 6. Schematic bifurcation diagram for the range $800 < R < 1050$. Results at higher R are not included because that regime was not studied in detail. The two horizontal lines are the asymmetric (top) and centrosymmetric limit cycles. ●, bifurcation points; ——, stable solutions; – – –, unstable solutions. Dotted curves (not encircled) are stable only in the centrosymmetric subspace. Instabilities of quasi-periodic flows are encircled; the resulting jumps between branches are indicated by arrows.

process. The section is divided into three parts. First, we discuss the observed changes in time dependence and construct a schematic bifurcation diagram, using results from a large number of simulations. Secondly, we present the spatial structures that arise at the instabilities found in the previous subsection. We also discuss the relation of these structures to the plume formation process and to the observed deviation from Howard scaling. Finally, we show how the observed results are related to the structure of the scaled governing equations and present a phase space scenario consistent with the behaviour.

5.1. *Bifurcation behaviour and time dependence*

We noted above that the 'bubble' of deviation from the boundary-layer scaling in figure 2 corresponds to a quasi-periodic flow. In this subsection, we describe this behaviour in more detail. The culmination of the discussion is a schematic bifurcation diagram showing a number of bubbles of quasi-periodic behaviour, corresponding to instabilities of two periodic flows of different wavenumbers (figure 6). We begin by considering only the space of centrosymmetric solutions, and later relax the constraint. The space of centrosymmetric solutions is invariant, so that connections to non-centrosymmetric branches can only occur via symmetry breaking bifurcations. Restriction to the centrosymmetric subspace allows the consideration of solutions that would otherwise be unstable, and thus allows the completion of the picture of one bubble of quasi-periodic behaviour. We use this case as a paradigm for the behaviour of the unconstrained system, where computational limitations prevent a complete picture from being resolved.

When $R = 925$ the centrosymmetric '$n = 9$' limit cycle (now with wavenumber 11, cf. §4) is linearly stable with respect to both centrosymmetric and non-centrosymmetric disturbances. We consider in this paragraph centrosymmetric deviations from this state. Between $R = 925$ and $R = 950$, the flow undergoes a supercritical torus bifurcation. At $R = 950$, with initial conditions from $R = 925$, a stable quasi-periodic state is found, with $f_1 = 404 \pm 2, f_2 = 176 \pm 2, \overline{Nu} = 10.80$. The frequency f_1 denotes the limit cycle frequency and f_2 the secondary frequency that arises at the bifurcation. Figure 7 shows the frequency spectra of $Nu(t)$ at $R = 950$ and $R = 1025$. The

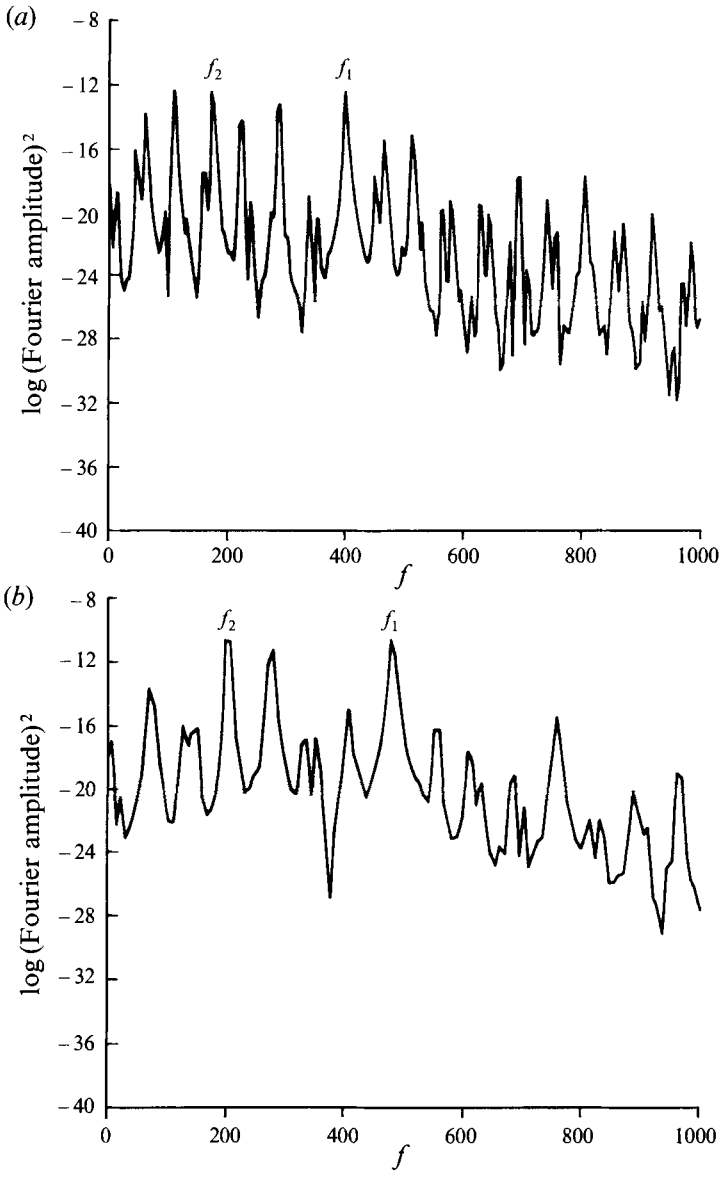

FIGURE 7. Spectra of Nu on the centrosymmetric quasi-periodic solution at (*a*) $R = 950$, (*b*) 1025.

bifurcation leads to a deviation from the boundary-layer behaviour, as $\overline{Nu}$ and f_1 fall below the interpolation of the Howard scaling behaviour. This disruption is especially clear on the curve of $\overline{Nu}$ *vs.* R on figure 2. Between $R = 950$ and $R = 975$, $\overline{Nu}$ actually decreases. As R increases, f_1 and f_2 evolve smoothly and f_2 remains close to $\frac{3}{7}f_1$. The deviation from locking is indicated by a low-frequency spectral peak. Between $R = 1025$ and 1040, the solution becomes periodic again as f_2 disappears. The variance of $Nu(t)$ in the quasi-periodic bubble is higher than in the periodic regimes on either side. As the flow becomes periodic again, f_1 and $\overline{Nu}$ resume the Howard scaling (figure 2). At $R = 1050$, the wavenumber has evolved to $n = 13$. The pair of torus bifurcations that bound this quasi-periodic regime can also be found directly by continuation methods.

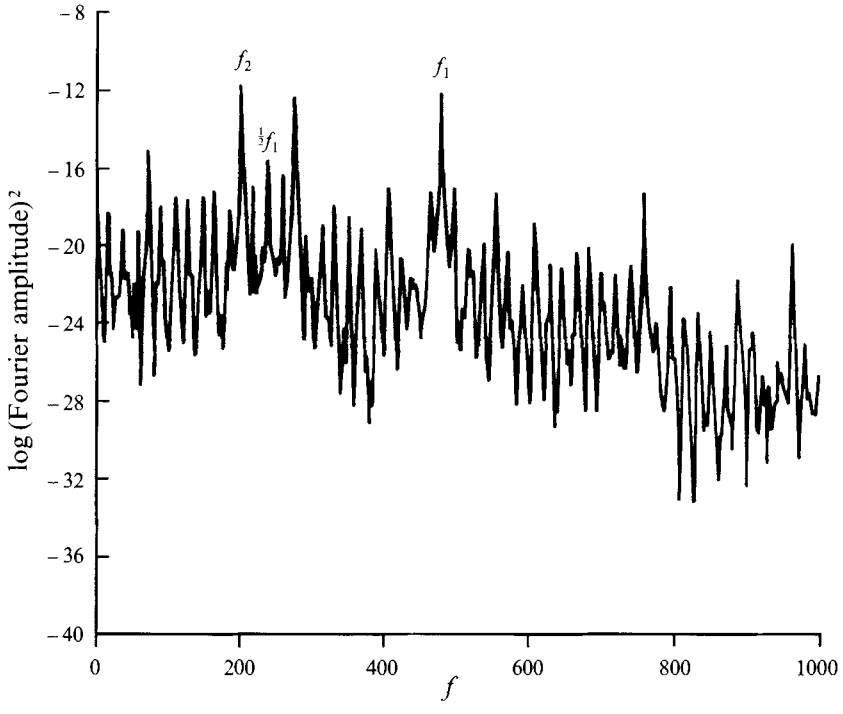

FIGURE 8. Spectrum of Nu on the non-symmetric quasi-periodic solution at $R = 1025$.

We now remove the constraint of centrosymmetry and find additional quasi-periodic behaviour similar to that found in the centrosymmetric space. A bubble of period-doubled solutions is found, as well a other quasi-periodic flows. These all disrupt the scaling behaviour, just as in the centrosymmetric case.

At $R = 925$ and $R = 1050$, the start and end points of the previous paragraph, the centrosymmetric limit cycle is stable in the unrestricted space. This discussion begins at $R = 1050$, and we proceed by reducing R. Reducing R to 1040 introduces the subharmonic $\frac{1}{2}f_1$ of the limit cycle frequency into the flow. Thus a subharmonic bifurcation occurs from the centrosymmetric limit cycle between $R = 1040$ and 1050.

Reducing R to 1025, the spectrum shows in addition to the subharmonic of f_1, the frequency f_2 corresponding to the centrosymmetric quasi-periodic (QP) state here. This non-centrosymmetric state is a mixed mode formed by interaction between the two branches. Locking occurs at $f_L = 16$ ($f_2 = 13f_L$, $\frac{1}{2}f_1 = 15f_L$); the harmonics of f_L are evident in the spectrum (figure 8). Upon decreasing R from 1025, f_1, f_2 and $\overline{Nu}$ remain close to the values on the centrosymmetric branch and the subharmonic persists (see figure 9). At $R = 1000$ the frequencies and $\overline{Nu}$ are close to those found by KSS, but they claim that the solution is chaotic. We find chaotic behaviour on this branch only if the resolution is insufficient. At $R = 975$, spectra of centrosymmetric and mixed states are distinguishable, but from initial conditions on the non-centrosymmetric QP solution, the Nusselt number evolution of the centrosymmetric and mixed states are virtually identical over at least $\frac{1}{8}$ of a diffusion time. That is, the mixed mode becomes more like the centrosymmetric state as R decreases. If R is decreased to 950, a drastic change in behaviour occurs. The solution jumps to a stable non-centrosymmetric limit cycle with a wavenumber $n = 12$. Thus, there exists a regime somewhere between $R = 925$ and 975, where the branch based on the centrosymmetric limit cycle is unstable with respect

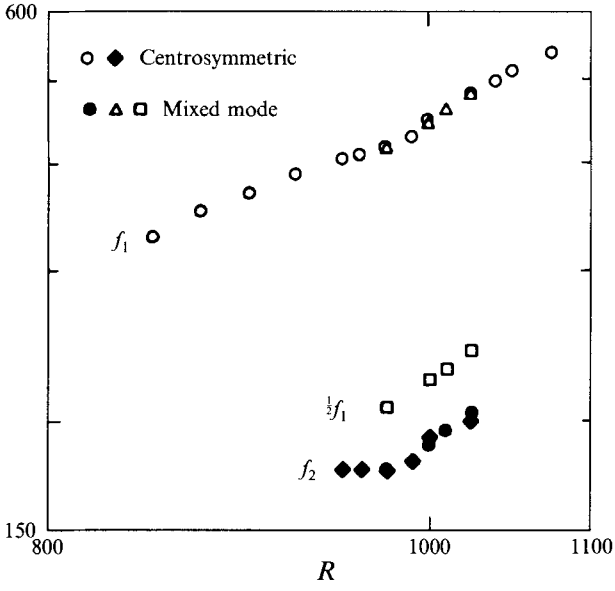

FIGURE 9. Frequencies of the centrosymmetric and mixed mode quasi-periodic solutions based on the centrosymmetric limit cycle.

to the non-centrosymmetric one. This regime of instability makes it impossible to determine exactly the fate of the subharmonic branch through IVPs. However, recall that at $R = 925$ the centrosymmetric limit cycle branch is linearly stable. At $R = 1050$ it is again linearly stable whereas at $R = 1040$, it is unstable to the subharmonic state. Therefore, a destabilizing bifurcation with an unstable manifold corresponding to the subharmonic structure must occur somewhere above $R = 925$. The presence of the mixed mode down to $R = 975$ suggests that the subharmonic branch simply rejoins the limit cycle, resulting in a second bubble. In principle, the subharmonic branch could be traced by continuation, although the computational cost of this would be prohibitive because the restriction to centrosymmetry could no longer be applied. Other scenarios are possible, but seem less plausible than the one above, both because the one above is the simplest and because the analogous scenario in the centrosymmetric subspace is observed directly.

We discuss briefly the behaviour on the non-centrosymmetric ($n = 12$) limit cycle branch found at $R = 950$. At $R = 1000$, the solution on this branch becomes quasi-periodic with $f_1 = 458$, $f_2 = 157$. KSS find a chaotic state with almost identical dominant frequencies; again the chaos is apparently due to insufficient resolution. At $R = 1025$, the solution is unstable, as the flow evolves toward the mixed mode quasi-periodic solution discussed above. Similar behaviour occurs as R is reduced from $R = 950$. At $R = 925$, the solution becomes weakly quasi-periodic (small variance in $Nu(t)$), at $R = 900$ the solution is strongly quasi-periodic (large variance) and at $R = 875$, the solution jumps back to the centrosymmetric limit cycle. By using a large step in R the stable non-centrosymmetric limit cycle can be found again at $R = 800$. As above, we conjecture that the quasi-periodic branch masked by instability is a simple bubble.

The above transitions are summarized in the schematic bifurcation diagram, figure 6. The diagram is not complete, as unstable non-centrosymmetric quasi-periodic solutions cannot be traced. However, the dotted lines (encircled) indicate where the bubble structure has been assumed, based on the arguments presented above. In §5.2,

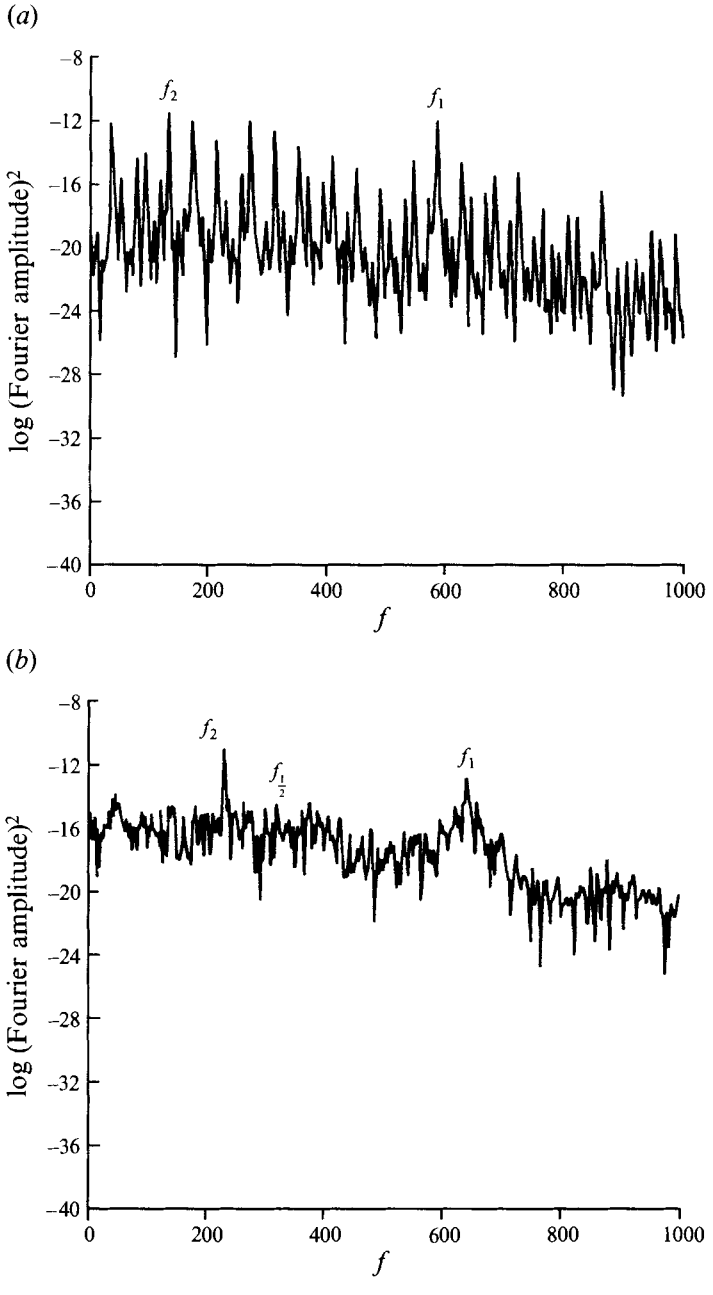

FIGURE 10. Spectra of Nu at (*a*) $R = 1150$, a quasi-periodic solution and (*b*) $R = 1200$, a chaotic one.

we show the similarities between the spatial structures that arise in these quasi-periodic regimes, further strengthening the analogy with the centrosymmetric case, where the bubble is found directly. Before discussing these structures, we describe some behaviour found at higher R.

The behaviour described in detail above persists at higher Rayleigh numbers and eventually weakly chaotic behaviour is observed. At $R = 1100$, a centrosymmetric quasi-periodic state born near $R = 1090$ becomes unstable to a quasi-periodic state

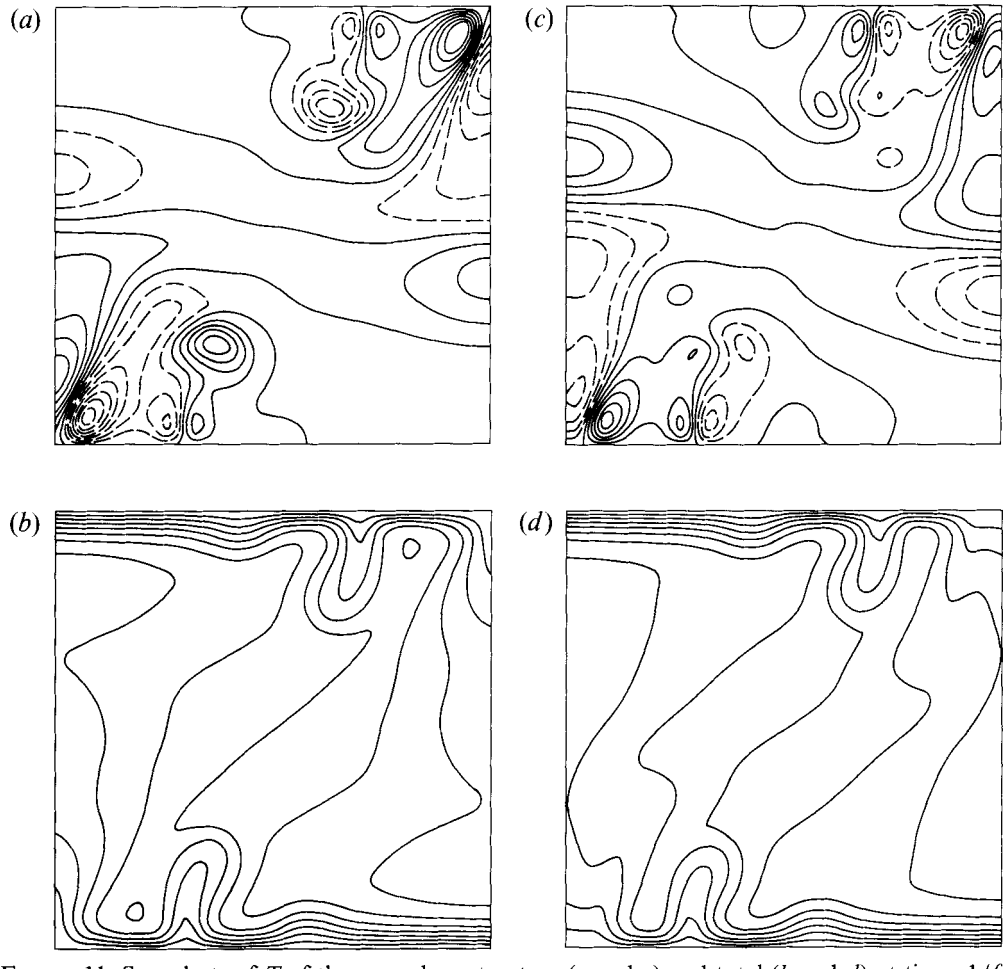

FIGURE 11. Snapshots of T of the secondary structure (a and c) and total (b and d) at times $1/f_1$ apart on the centrosymmetric quasi-periodic solution at $R = 950$.

based on the asymmetric limit cycle. A similar solution is found at $R = 1150$ and weakly chaotic solutions are found at $R = 1200$ and 1250. Figure 10 displays spectra of a quasi-periodic solution at $R = 1150$ and a chaotic one at $R = 1200$. The length of the time series and number of samples are identical in the two cases. The difference in background level clearly shows the distinction between quasi-periodic and chaotic signals. The chaotic motion occurs via period doubling, as frequencies $\frac{1}{4}f_1$, $\frac{1}{2}f_1$ and $\frac{3}{4}f_1$ are discernible in the spectrum at $R = 1200$ and f_2 is close to $\frac{3}{8}f_1$.

Care has been taken to assure that the chaotic solution at $R = 1200$ is not spurious. With 48 Chebyshev polynomials in the vertical direction, giving grid spacings of $O(5 \times 10^{-4})$ in the boundary layers, vertical resolution is more than sufficient. Runs with 72, 80 and 84 Fourier modes in the horizontal direction all give spectra with similar structures. The peaks at $f_1 = 640$ and $f_2 = 232$ persist at all three truncations.

5.2. *Spatial structures and physical processes*

As discussed above, the onset of Howard scaling corresponds to the formation of plumes. Thus, on physical grounds it is expected that deviation from these scaling laws is associated with disruption of the plume formation process, i.e. some change in the

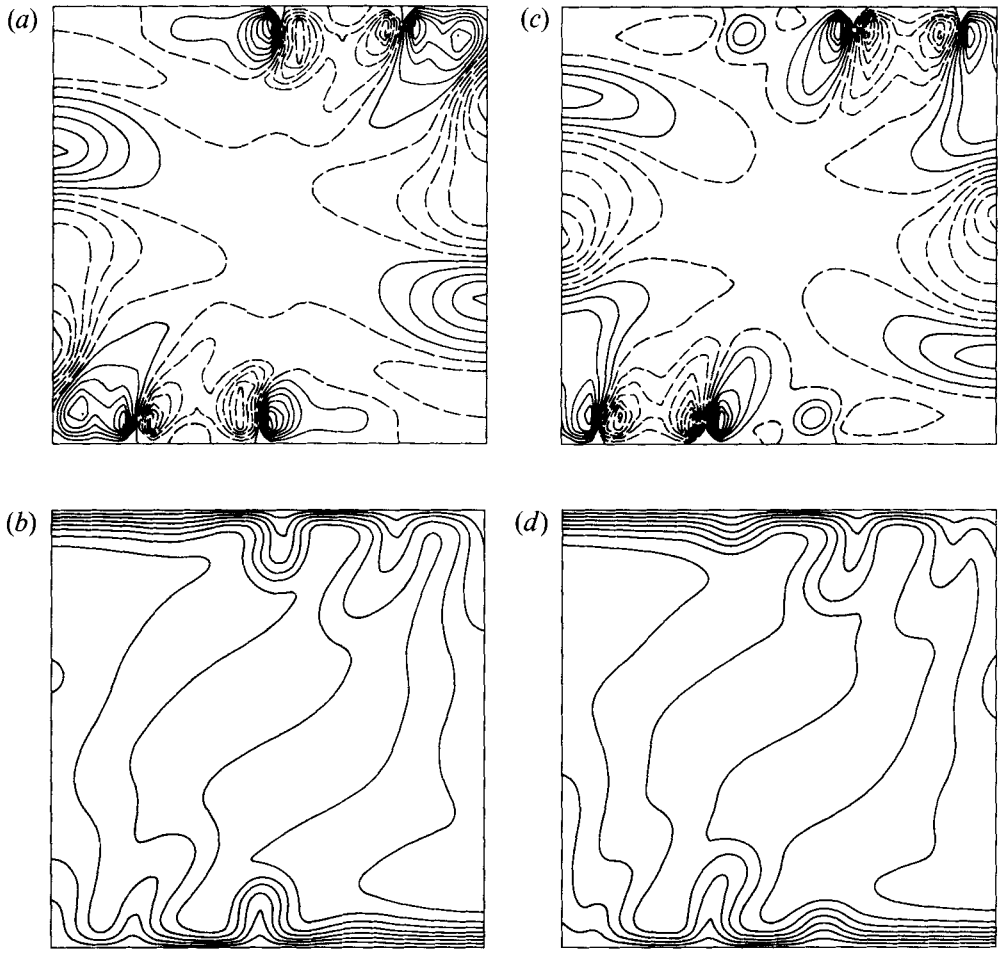

FIGURE 12. Snapshots of T: the subharmonic secondary structure (a and c) and total (b and d) at times $1/2f_1$ apart on the subharmonic solution at $R = 1040$.

dynamics of the boundary layers. One possible source of such a disruption can be seen in figure 4, where a fluctuation in a plume originating in, say, the bottom boundary layer may be strong enough to distort the upstream end of the top boundary layer, where cold plumes begin to form. In short, disruption of Howard scaling represents communication between top and bottom because the heat transfer now depends on top to bottom distance. In this subsection, we illustrate the changes in the spatial structures that are associated with quasi-periodicity and the deviation from scaling. These secondary structures are obtained by Fourier analysing the original temperature fields in time, filtering out the mean, the plume formation frequency and its harmonics and displaying the remainder.

Figure 11 shows the instantaneous temperature field and the secondary structure (the primary structure being that of the periodic plume formation) at two instants $1/f_1$ apart for the centrosymmetric quasi-periodic flow at $R = 950$. Extrema in the magnitude and gradients of the secondary structure occur exactly at the positions of the plumes and travel with the plumes. In addition, the disturbance changes sign on a curve that passes vertically through each plume. This locus of sign-change effectively shifts the horizontal position of each plume, so with each plume formation cycle the

plumes differ slightly in position relative to one another; each plume forms slightly upstream or downstream of the mean position of formation. In essence, then, the instability is a phase modulation of the plume formation process. This point will be discussed further in the next section.

Very similar structures arise in all of the other quasi-periodic bubbles. Figure 12 shows the secondary structure at $R = 1040$. This structure is invariant under rotation by π, apparently a manifestation of the resonance phenomenon causing the subharmonic bifurcation. This is not a centrosymmetric fluctuation, as centrosymmetry is defined as invariance under rotation by π and sign change. The plume formation process is simpler here than in the case at $R = 950$. When the flow is simply periodic, every plume is identical, modulo a shift in time. In this subharmonic case, every other plume is identical. In truly quasi-periodic cases, no two plumes are identical. The results for the mixed mode and the quasi-periodic flows based on the non-centrosymmetric limit cycle are very similar (Graham 1992). A similar structure is also found in the chaotic flow at $R = 1200$. Figure 13 shows snapshots of the secondary and total structures at $R = 1200$. The secondary structure is similar to those at lower R, except that large amplitudes are present further upstream in the boundary layers. This is consistent with the structures at lower R, because plumes form further upstream as R increases.

5.3. *Instability mechanism and nonlinear dynamics*

The bifurcations and associated physical structures described above are not observed at lower Rayleigh number, where boundary-layer plumes are absent. However, before considering the regime of plume formation, it is instructive to review the dynamics of the lower Rayleigh number regimes. Plume production may be regarded as one stage in an evolving struggle between horizontal and vertical lengthscales for dominance of the overall (vertical) heat transport.

In the steady convection regime Robinson & O'Sullivan (1976) have shown that horizontal convection balances diffusion where the time for travel across the bottom of the box $t \sim R^{-\frac{2}{3}}$. Furthermore, $\delta \sim R^{-\frac{2}{3}}$ which gives $\overline{Nu} \sim R^{\frac{2}{3}}$. Steady convection is unstable to travelling waves. The base state velocity convects thermal disturbances around a loop for these waves. The spatial structure of the disturbance (wavenumber n) is determined primarily by a balance of diffusion in the loop direction with convection (Steen & Aidun 1988). The relevant timescale is the time for a disturbance to sweep across the bottom (or top). The corresponding travelling wave or 'sweep' frequency is $f \sim nR^{\frac{7}{6}}$. It is observed that n is invariant along branches in this regime (GS). There, periodic motions compete with quasi-periodic motions and the dynamic behaviour is understood in terms of coupled nonlinear oscillators of nearly the same strength. The end of this regime occurs as vertical transport in the boundary layers begins to dominate horizontal transport. This also marks the beginning of the next regime, the Howard scaling regime. It has particularly simple scaling properties since δ is independent of box size, as outlined above. The dominant balance is between vertical diffusion and unsteadiness close to the isothermal boundaries. One feature of this balance is that wavenumber is no longer preserved along branches. For example, a smooth transition from an $n = 11$ to $n = 13$ wavenumber occurs, as pointed out above.

We now focus on the regime of Howard scaling and deviations from it ($700 < R < 1200$). The base state is the time-periodic flow of the $n = 9/11/13$ branch and satisfies

$$\frac{\partial \bar{\theta}}{\partial t} = \nabla^2 \bar{\theta} - \bar{v} \cdot (\nabla \bar{\theta} - \boldsymbol{k}). \tag{14}$$

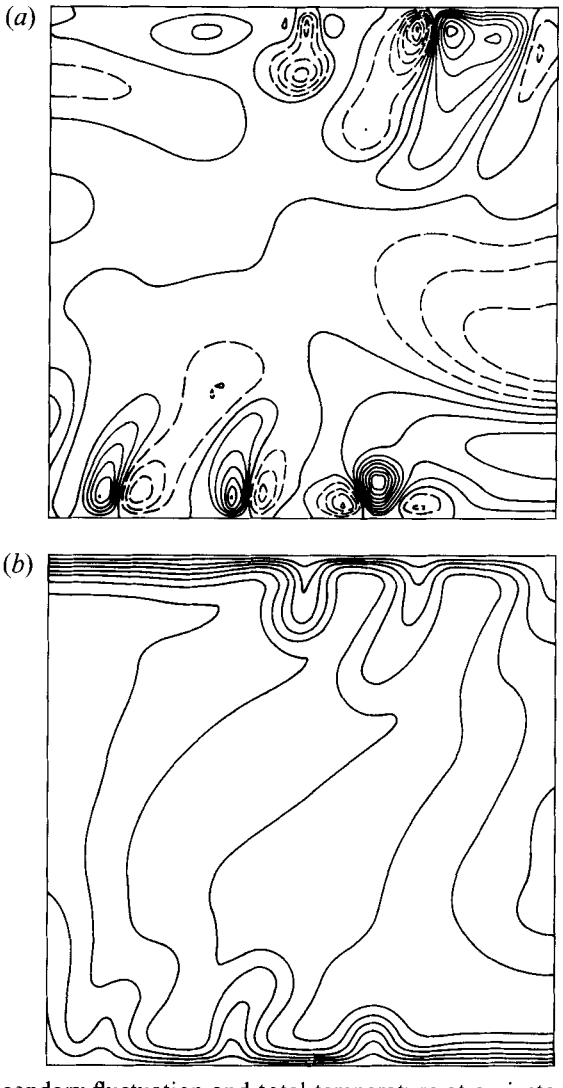

FIGURE 13. Secondary fluctuation and total temperature at an instant, $R = 1200$.

Consistent with the above discussion of the scaling laws,

$$\bar{v} \sim O(R), \quad \nabla\bar{\theta} \sim O(R), \quad f_1 \sim O(R^2).$$

The relevant timescale for the periodic base state is the plume frequency f_1. However, we expect that the sweep frequency, which now varies as $1/\bar{v} \sim R^{-1}$, is the relevant timescale for the instability. Using the above expressions to rescale the periodic solution and time, the linearized disturbance energy equation becomes

$$R\frac{\partial\hat{\theta}}{\partial t} = -R\{\bar{v}\cdot\nabla\hat{\theta} + \hat{v}\cdot\nabla\bar{\theta}\} + \{\nabla^2\hat{\theta} - \hat{v}\cdot k\}. \tag{15}$$

This result suggests that the convective and time dependent contributions to the disturbance equation provide the dominant balance, and are $O(R)$ larger than the dissipative term, except where very steep gradients exist in $\hat{\theta}$. From the plots of the secondary structures, it can be seen that steep gradients are very localized, so in

general, the above ordering of terms is valid. As R is increased, the plume and sweep frequencies come into resonance, $f \sim f_1$, near the bubble of deviation from Howard scaling. This is consistent with the appearance of a second frequency $f_2 \sim \frac{1}{2}f_1$, typical of parametric resonance (see e.g. Nayfeh & Mook 1979). The time-periodic coefficients in the linearized disturbance equations represent an oscillator whose strength has grown with Rayleigh number since inception ($R = 544$) and which is now strong enough, in contrast to its role at lower R, to be a forcing oscillator. Parametric instability occurs.

To understand this resonance better, we attempt to identify a mechanism for the process. One timescale is the time for the plume formation process, $1/(f_1)$, which is $O(R^{-2})$. The second important timescale is the sweep time across the top and bottom which is $O(R^{-1})$ and in dimensional terms depends on l. The ratio between sweep time and plume formation time changes continuously with R. At lower R where plume formation is very weak, the sweeping action entrains the plumes. At higher R, as the system moves in and out of timescale ratios where it is susceptible to resonance, instabilities can ensue. One can imagine that the instability process occurs like this: a fluctuation in the bottom boundary layer causes a plume to form just a little bit early causing a horizontal compression of the wavetrain (and vertical expansion). This leads to two plumes being slightly closer to each other than they would otherwise be. These two plumes together do a slightly better job of cleaning cold fluid of the boundary layer than usual. This leads to a little longer induction time for the next plume to form, a larger interval between plumes and a slightly worse job of cleaning out the boundary layer. Thus the next plume forms a little early and the flow develops a phase-modulated train of disturbances. If the timing of the intervals between disturbances in the wavetrain resonates with the timing of plume formation, a phase modulated state is sustained around the loop. The average effect is a decrease in the heat transfer. A variant of this mechanism views the plume modulation as due to direct communication from bottom to top across the box (and vice versa), not through the wavetrain around the loop. In either case, as R increases further, the frequencies move out of resonance, the plumes strengthen and accordingly their physics dominates. Again, f_1 emerges as the only relevant timescale at higher R (until the next resonance occurs).

Lennie *et al.* (1988) find somewhat similar behaviour in their simulations of convection of a volumetrically heated fluid cooled from above. In a rectangular container with aspect ratio (horizontal size to vertical size) $h = 1.5$, the single roll steady state is destabilized at a Hopf bifurcation, above which two cold blobs circulate with the bulk flow. At a period-doubling bifurcation, one of these blobs becomes more prominent than the other; they interpret this change as a resonant spatial modulation of the blob structure, an amplitude modulated wave. They then draw analogies with the work of Rand (1982), who discusses modulated travelling waves in the fully symmetric context of rotating flows. There is then a period-doubling cascade to chaos, followed by a reverse cascade leading back to the same periodic branch from which the sequence started. In short, they find a bubble of subharmonic (and more complicated) behaviour superficially similar to what we find here. However, they do not analyse the spatial structures in detail, so their results cannot be directly compared with ours. Furthermore, we observe phase modulation rather than amplitude modulation; nevertheless their results are, to our knowledge, the most closely related to ours that have been found.

Finally, we discuss a possible phase space scenario for the jumps from the quasi-periodic branches. The scenario is not unique in describing the observed behaviour, but it is, we believe, the simplest. The new quasi-periodic structures have a tendency to be

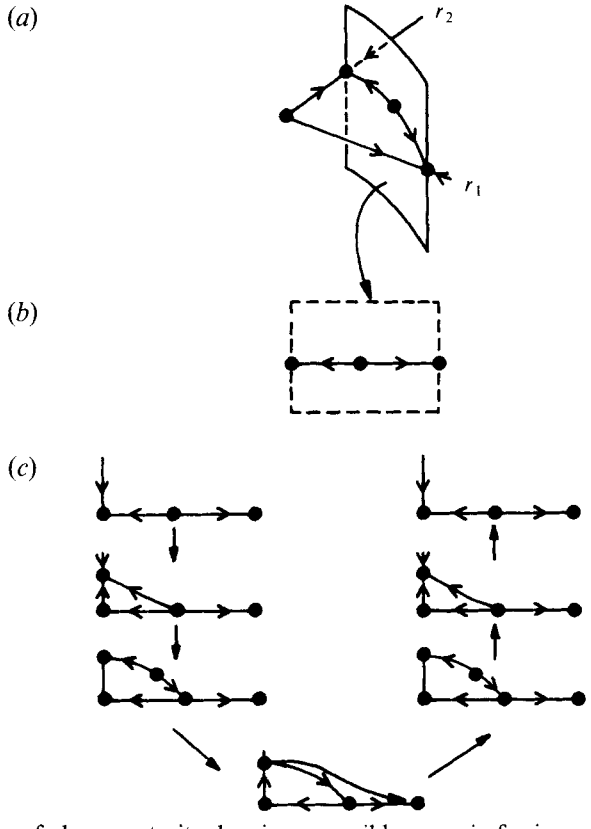

FIGURE 14. A sequence of phase portraits showing a possible scenario for jumps between limit cycle-based solutions. (*a*) The orientation of the limit cycles. The origin is the unstable steady roll. (*b*) The limit cycles and unstable mixed mode on a horizontal axis representing the separatrices connecting them. (*c*) A sequence of bifurcations. The vertical axis represents the amplitude of a secondary (quasi-periodic) disturbance structure.

unstable, as jumps from these states to states based on the other limit cycle have occurred in every case. Perhaps it is because they reduce heat transfer efficiency, allowing perturbations to grow. Regardless of the physical mechanism, it appears that all jumps are associated directly with instabilities of quasi-periodic states, not of the limit cycles themselves. At $R = 800$, both the centrosymmetric and non-centrosymmetric limit cycles are stable, so locally, the phase space (of oscillation amplitudes) appears as shown in figure 14(*a*). The origin is the steady one-roll state, the two limit cycles are on the axes and are separated by an unstable mixed-mode quasi-periodic solution. Figure 14(*b*) shows the limit cycles and mixed mode on a horizontal axis corresponding to the separatrices connecting the mixed mode to the limit cycles. This mixed mode is due to the interaction between limit cycles (cf. GS), not tori, and should not be confused with the mixed mode of the previous section. The vertical axis on this figure represents the amplitude of secondary Hopf (torus) bifurcations discussed above. Figure 14(*c*) shows a possible bifurcation scenario. A quasi-periodic solution is born from one of the limit cycles. It interacts with the mixed mode and becomes unstable at large amplitude, thus causing the jump to the alternate limit cycle. As R increases further, the amplitude decreases and the quasi-periodic solution regains stability, finally vanishing again, leaving the limit cycle stable. This scenario is applicable to all of the quasi-periodic bubbles found.

6. Conclusion

The Rayleigh number regime studied here ($600 < R < 1250$) is characterized by thermal plumes and overall follows the classical high R asymptotic scaling behaviour. The plumes drive resonant instabilities that lead to windows of quasi-periodic, subharmonic or weakly chaotic behaviour. The plume formation process is disrupted in these windows, causing deviations from the simple scaling behaviour. These deviations may actually decrease $\overline{Nu}$ as R increases. The instability is essentially a phase modulation of the plume formation process. To our knowledge, resonant bifurcations giving windows of quasi-periodic behaviour have not been previously observed in either pure fluid or porous media convection.

The model of Howard predicts a single characteristic frequency, the rate of plume formation. It is interesting to ask how this model and frequency are related to the multiple frequencies and broadband spectra associated with quasi-periodicity, chaos and turbulence in convection. This study implicitly gives a partial answer to this question. The plumes that are an essential component of the model are not independent from each other, but interact nonlinearly and in the present case resonantly. A better understanding of the phenomena described here may prove important in understanding the dynamics of plumes in convection at even higher R.

This work was partially supported by NSF/AFOSR DMS-8915672. Simulations were conducted using the Cornell National Supercomputer Facility, a resource of the Center for Theory and Simulation in Science and Engineering at Cornell University, which receives major funding from the National Science Foundation and the IBM Corporation, with additional support from New York State and members of the Center's Corporate Research Institute.

REFERENCES

AIDUN, C. K. & STEEN, P. H. 1986 Transition to unsteady convective heat transfer in a fluid-saturated porous medium. *AIAA/ASME 4th joint Thermophysics and Heat Transfer Conf., AIAA Paper* 86–1264.

AIDUN, C. K. & STEEN, P. H. 1987 Transition to oscillatory convective heat transfer in a fluid-saturated porous medium. *J. Thermophys. H.T.* **1**, 268–273.

BECK, J. L. 1972 Convection in a box of porous material saturated with fluid. *Phys. Fluids* **15**, 1377–1383.

BOYD, J. P. 1989 *Chebyshev and Fourier Spectral Methods.* Springer.

BURETTA, R. J. 1972 Thermal convection in a fluid filled porous layer with uniform internal heat sources. PhD thesis, University of Minnesota.

CALTAGIRONE, J.-P. & FABRIE, P. 1989 Natural convection in a porous medium at high Rayleigh numbers Part I – Darcy's model. *Eur. J. Mech.* B **8**, 207–227.

CANUTO, C., HUSSAINI, M. Y., QUARTERONI, A. & ZANG, T. A. 1988 *Spectral Methods in Fluid Dynamics.* Springer.

CASTAING, B., GUNARATNE, G., HESLOT, F., KADANOFF, L., LIBCHABER, A., THOMAE, S., WU, X.-Z., ZALESKI, S. & ZANETTI, G. 1989 Scaling of hard thermal turbulence in Rayleigh–Bénard convection. *J. Fluid Mech.* **204**, 1–30.

DOEDEL, E. J. 1981 AUTO: a program for the automatic bifurcation analysis of autonomous systems. *Congress Numerantum* **30**, 265–284, 1981 (*Proc. of the 10th Manitoba Conf. on Numerical Mathematics and Computation, University of Manitoba, Winnepeg, Canada, 1980*).

DRAZIN, P. G. & REID, W. H. 1981 *Hydrodynamic Stability.* Cambridge University Press.

ELDER, J. W. 1967 Steady free convection in a porous medium heated from below. *J. Fluid Mech.* **27**, 29–48.

ELDER, J. W. 1968 The unstable thermal interface. *J. Fluid Mech.* **32**, 69–96.

FORNBERG, B. 1990 An improved pseudospectral method for initial-boundary value problems. *J. Comput. Phys.* **91**, 381–397.

FOSTER, T. D. 1965 Stability of a homogeneous fluid cooled uniformly from above. *Phys. Fluids* **8**, 1249–1257.

GRAHAM, M. D. 1992 Dynamics and mechanisms of time-dependent natural convection in porous media. PhD thesis, Cornell University.

GRAHAM, M. D. & STEEN, P. H. 1992 Strongly interacting traveling waves and quasiperiodic dynamics in porous medium convection. *Physica* D **54**, 331–350.

HAIDVOGEL, D. B. & ZANG, T. 1979 The accurate solution of Poisson's equation by expansion in Chebyshev polynomials. *J. Comput. Phys.* **30**, 167–180.

HORNE, R. N. & O'SULLIVAN, M. J. 1978 Origin of oscillatory convection in a porous medium heated from below. *Phys. Fluids* **21**, 1260–1264.

HOWARD, L. N. 1964 Convection at high Rayleigh number. *Applied Mechanics, Proc. 11th Cong. Appl. Mech.* (ed. H. Görtler), pp. 1109–1115.

JOSEPH, D. D. 1976 *Stability of Fluid Motions II.* Springer.

KIMURA, S., SCHUBERT, G. & STRAUS, J. M. 1986 Route to chaos in porous-medium thermal convection. *J. Fluid Mech.* **116**, 305–324.

KIMURA, S., SCHUBERT, G. & STRAUS, J. M. 1989 Time-dependent convection in a fluid-saturated porous cube heated from below. *J. Fluid Mech.* **207**, 153–189.

KOSTER, J. N. & MÜLLER, U. 1982 Free convection in vertical gaps. *J. Fluid Mech.* **125**, 429–451.

KRISHNAMURTI, R. 1979 On the transition to turbulent convection. Part 2. The transition to time-dependent flow. *J. Fluid Mech.* **42**, 309–320.

LENNIE, T. B., MCKENZIE, D. P., MOORE, D. R. & WEISS, N. O. 1988 The breakdown of study convection. *J. Fluid Mech.* **188**, 47–85.

NAYFEH, A. H. & MOOK, D. T. 1979 *Nonlinear Oscillations.* Wiley.

RAND, D. A. 1982 Dynamics and symmetry: predictions for modulated waves in rotating fluids. *Arch. Rat. Mech. Anal.* **79**, 1–37.

ROBINSON, J. L. & O'SULLIVAN, M. J. 1976 A boundary-layer model of flow in a porous medium at high Rayleigh number. *J. Fluid Mech.* **75**, 459–467.

STEEN, P. H. 1986 Container geometry and the transition to unsteady Bénard convection in porous media. *Phys. Fluids* **29**, 925–933.

STEEN, P. H. & AIDUN, C. K. 1988 Time-periodic convection in porous media: transition mechanism. *J. Fluid Mech.* **196**, 263–290.

TURNER, J. S. 1973 *Buoyancy Effects in Fluids.* Cambridge University Press.